Appl. Phys. B 73, 165–172 (2001) / Digital Object Identifier (DOI) 10.1007/s003400100626

Applied Physics B
Lasers
and Optics

Hydrogen CARS thermometry in a high-pressure H_2–air flame. Test of H_2 temperature accuracy and influence of line width by comparison with N_2 CARS as reference

J. Hussong[1], R. Lückerath[1], W. Stricker[1,*], X. Bruet[2], P. Joubert[2], J. Bonamy[2], D. Robert[2]

[1] DLR Institut für Verbrennungstechnik, Postfach 800 320, 70503 Stuttgart, Germany
[2] Laboratoire de Physique Moléculaire, UMR CNRS 6624, Université de Franche-Comté, 25030 Besançon Cedex, France

Received: 10 April 2001/Revised version: 22 May 2001/Published online: 18 July 2001 –

Abstract. This work describes a further step towards the determination of the temperature accuracy of H_2 Q-branch CARS (Coherent Anti-Stokes Raman Scattering) at high pressure with regard to the influence of the H_2 line widths. In laminar steady H_2/air flames in the pressure range 1–15 bar and at fuel-rich conditions with stoichiometries between two and four, quasi-simultaneous temperature measurements were performed with H_2 and N_2 CARS. The temperature values deduced from H_2 CARS are in good agreement with the reference temperature from N_2 CARS. The influence of different line-width contributions on the accuracy of H_2 Q-branch thermometry was investigated in detail.

PACS: 33.20.Fb; 33.70.Jg; 42.65; 82.40.Py

For the study of cryogenic H_2-O_2 combustion as in rocket engines the accurate determination of temperature is of great importance in order to better understand atomization, mixing, and flame stability. Under the harsh boundary conditions of high-pressure H_2-O_2 combustion, frequently linked in the laboratory with large distances due to safety precautions and with short time periods of operation, CARS thermometry has the most promising potential as a diagnostic tool. As thermometer species, H_2O and H_2 can be considered. H_2O, however, is of minor importance, mainly for two reasons. First, H_2O as the combustion product is not present in all regions of the combustor and thus this limits the accessible temperature range. Second, due to the lack of precise molecular data on line frequencies and line widths at high temperature, H_2O is the less reliable temperature-indicator species. In contrast, H_2 as fuel is used in excess for reasons of stability and therefore present in all areas of the combustion chamber. For thermometry in practical air-fed combustion, N_2 CARS has proven to be a matured and established method, since an accurate description of the Q-branch spectrum is possible, based on accurate molecular constants and line-width data. This is not the case for H_2 thermometry. Although H_2 has been used for CARS thermometry for several years, no systematic investigation has been carried out to determine the accuracy of H_2 CARS temperature in the high-pressure regime, where the influence of line broadening is important. Hancock et al. [1] performed CARS temperature measurements using N_2 and H_2 in an atmospheric pressure H_2/air flame, stabilized on a near-adiabatic, surface-mixing Hencken burner. They observed a systematic deviation between the temperatures derived from N_2 and H_2 CARS Q-branch spectra, respectively, for fuel-rich conditions. Assuming that the N_2 temperatures are the more reliable ones, the deviations are probably due primarily to uncertainties in H_2 line widths and line-broadening mechanisms. For the case of H_2 as a minor species in the exhaust of a fuel-rich, high-pressure CH_4/air flame Bergmann et al. [2, 3] proposed an energy-corrected sudden (ECS) scaling law as an empirical model for the calculation of H_2 line widths for pressures up to 40 bar. The evaluated H_2 Q-branch CARS temperatures were in very good agreement with the reference temperature obtained independently by spontaneous Raman scattering of N_2.

In the work reported here a systematic study has been performed to address the accuracy of temperature measurements from Q-branch spectra of H_2 as a majority component in laminar, premixed high-pressure flames. As the stabilization of premixed H_2/O_2 flames is very difficult, H_2/air flames have been investigated. Dilution by N_2 yielded a reduced burning velocity and a lower flame temperature, which allowed the operation of the high-pressure flame for approximately one hour without the danger of destroying the flame holder and the burner by too large heat losses to the burner plate. This time was sufficient to carry out several sets of experiments. In addition, burning the flame with air as oxidizer made it possible to use N_2 for temperature measurements as a reference. However, the presence of N_2 complicates the description of the H_2 line widths, because for H_2-N_2 mixtures inhomogeneous line broadening by speed effects has to be considered [4]. The influence of these effects on H_2 CARS thermometry has been studied previously for H_2-N_2 mixtures at high-pressure and medium temperatures [5]. For temperature measurements in H_2/air flames, essentially three species contribute to the broadening of the H_2 Raman lines: H_2 (as a majority species at fuel-rich stoichiometries), N_2 (as

*Corresponding author. (E-mail: winfried.stricker@dlr.de)

inert species from air) and H_2O (as the reaction product). This means that the line-broadening mechanisms of the collision systems H_2-H_2, H_2-N_2, and H_2-H_2O have to be known. Due to the speed effects by N_2 as collider, it is not possible to employ the common linear mixing rule to deduce ternary mixture pressure-broadening coefficients from those obtained from binary ones.

Temperature measurements have been performed for three stoichiometries and various pressures using both H_2 and N_2 as probe molecule. To obtain an accurate temperature from N_2 CARS, the pressure-broadening coefficients for a large range of the rotational quantum number J in the N_2-N_2, N_2-H_2 and N_2-H_2O systems are needed, too.

The experimental set-up is described in Sect. 1. The way the N_2 and H_2 CARS spectra are calculated is explained in Sect. 2, with particular emphasis on the pressure-broadening coefficients. Results of the flame experiments and a comparison between H_2 and N_2 temperatures are discussed in Sect. 3.

1 Experimental set-up

The experimental set-up used for these investigations was similar to that employed in an earlier study [5]. Therefore, only a short description is given here. To enable the application of H_2 and N_2 CARS (quasi-) simultaneously on the same flame, two independent laser systems were used. For the N_2 CARS measurements our mobile CARS apparatus [6] was placed near the high-pressure burner (Fig. 1) in an adjacent room. The mobile CARS system is remotely controlled; thus a safe operation was insured while the burner was pressurized. The apparatus consists of a frequency-doubled Q-switched Nd:YAG laser (Spectra Physics DCR 4) with a donut-beam profile to serve as the pump source for the N_2 CARS process and the broadband dye laser. The N_2 CARS system delivers laser light at about 140 mJ/pulse at 532 nm and 14 mJ/pulse at 607 nm in a USED-CARS [7] arrangement. For the H_2 CARS experiments a single-mode Nd:YAG laser (Spectra Physics GCR 230) was used as the pump source for both the H_2 CARS process and the Stokes laser (modeless dye laser, ModeX) [5]. The Nd:YAG laser was operated in the oscillator mode only. 100 mJ/pulse was used to pump the dye laser (pyridine I and DCM, dissolved in methanol) and about 10 mJ/pulse for the CARS pump beam. The dye-laser output was about 9 mJ/pulse at a central wavelength of 680 nm (FWHM = 12 nm). Here, a folded BOXCARS arrangement [7] was employed. Both lasers were focused by lenses of $f = 200$-mm focal length into the flame. The spatial resolution of both CARS set-ups was experimentally determined to be 2.5 mm for the N_2 system and 0.6 mm for the H_2 system, defined as the length along which 95% of the signal is generated. The different numerical values are caused by the focusing properties of the USED CARS and BOXCARS geometries. However, both values are small enough to insure a homogeneous probe volume in the center of the flame.

To enable the measurement of axial temperature profiles, the exciting laser beams of the N_2 system were passed over two motor-driven, computer-controlled translation stages. For experimental reasons it was not possible to measure H_2 and N_2 CARS spectra really simultaneously, but due to the fast and precise change of the two optical pathways both H_2 and N_2 CARS spectra could be recorded successively within a time delay of less than 1 min, which should be sufficient for the laminar, stable flame. The signals were imaged onto

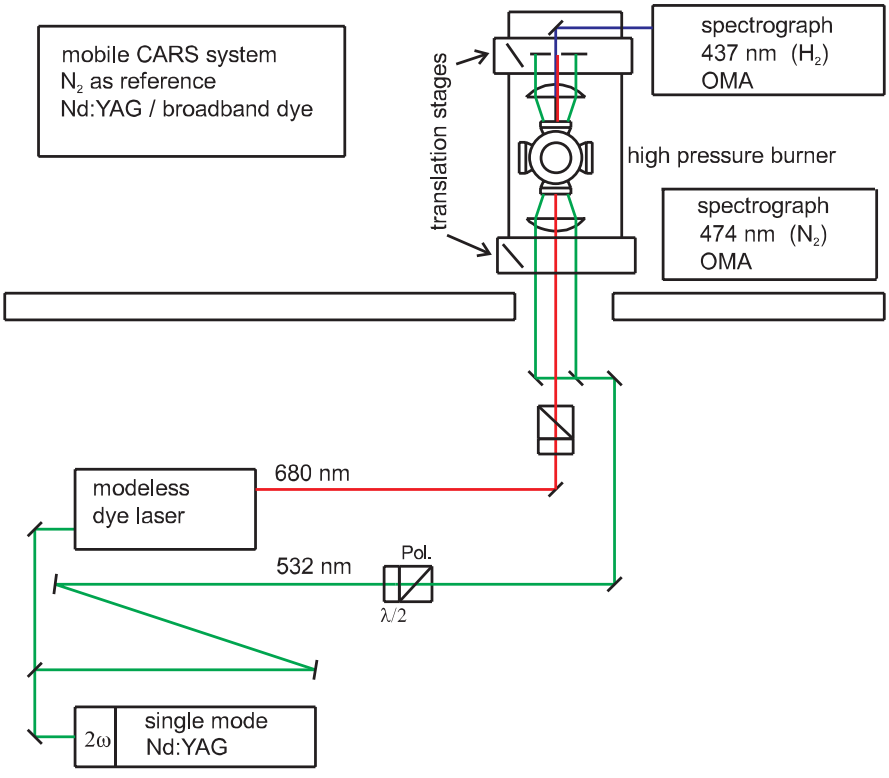

Fig. 1. Experimental set-up

the entrance slits of two spectrographs and detected by one-dimensional diode arrays.

To insure the necessary, well-defined conditions in the probe volume laminar, premixed, fuel-rich H_2/air flames were stabilized on a sintered bronze matrix, 8 mm in diameter, yielding a quiet, flat flame front less than 1 mm above the burner surface. The CARS measurements were performed in the homogeneous post-reaction zone. The housing of the burner was equipped with four windows, 12 mm in diameter, to provide optical access. Because of the particular properties of H_2/air flames (very high temperature and flame velocities) no additional heating of the flame holder and the burner nozzle (to avoid condensation of water inside the burner) was necessary, in contrast to hydrocarbon/air flames. Due to the large heat load to the burner matrix it was advisable to monitor the temperature of the burner head by a thermocouple in order to achieve the safe operation of the H_2/air flames without the risk of destroying the burner. Nevertheless, the flame stability was a critical issue, and there was only a small range of stoichiometry around $\Phi = 4$, where the temperature rise of the flame holder was about 1–3 degree per minute. The measurements were performed at stoichiometries of $\Phi = 3.8$ at 14 bar and $\Phi = 3.6$ at 15 bar. The temperature of the exhaust nozzle was fixed by heat-exchanging oil to about 130 °C. Figure 1 gives a view of the experimental set-up.

2 Computation of H_2 and N_2 CARS spectra

2.1 H_2 CARS spectra

The previous study in a cell for H_2-N_2 mixtures showed that, due to the limited spectral resolution of the broadband CARS detection scheme, it was sufficient to describe the H_2 line shape by a Lorentzian profile, even when inhomogeneous broadening effects cause a significant asymmetry contribution to the line profile for the case of high concentrations of the perturber [4]. The molecular line shape in the Q-branch CARS spectrum for the ternary mixture can then be written as a sum of isolated symmetric lines

$$I_{\mathrm{CARS}}^{\mathrm{H_2}} \propto \left|\chi_R^{(3)}\right|^2 = \left|\frac{N}{\hbar^3}\sum_{\mathrm{J}} \times \frac{g_{\mathrm{J}}\alpha_{\mathrm{J}}^2(2\mathrm{J}+1)\,\mathrm{e}^{E_{\mathrm{J}}/kT}(1-\mathrm{e}^{-E_{\mathrm{v=1}}/kT})}{\omega_{\mathrm{J}}-\omega_{\mathrm{P}}+\omega_{\mathrm{S}}+\Delta_{\mathrm{J}}(C_{\mathrm{N_2}},C_{\mathrm{H_2O}};T)-i\Gamma_{\mathrm{J}}(C_{\mathrm{N_2}},C_{\mathrm{H_2O}};T)}\right|^2 \tag{1}$$

In (1), N is the number density of the Raman-active molecules, α_{J} is the molecular polarizability, E_{J}, $E_{\mathrm{v=1}}$, ω_{P} and ω_{S} are the rotational energy of the state J, the energy of the first vibrational state, the pump and the Stokes frequencies, respectively. Γ_{J} is the line width and Δ_{J} the line shift of the Raman transition J depending on the gas composition and temperature. For broadband CARS it has been shown [5] that the relevant factor for the determination of the temperature is the integrated intensity of the most intense lines in the H_2 Q-branch spectrum. Since this value is proportional to $(\Gamma_{\mathrm{J}})^{-1}$ [8] and independent of Δ_{J}, the line shift can be neglected. But it has also been shown that the precision of the line widths is important for obtaining a high accuracy of the temperature measurement. These line widths are written as a sum of two terms: the Dicke narrowing [9, 10] and the collisional broadening

$$\Gamma_{\mathrm{J}}(C_{\mathrm{N_2}},C_{\mathrm{H_2O}};T) = \frac{2\pi D_0(C_{\mathrm{N_2}},C_{\mathrm{H_2O}};T)\omega_{\mathrm{J}}^2}{c\varrho} + \gamma_{\mathrm{J}}^0(C_{\mathrm{N_2}},C_{\mathrm{H_2O}};T)\varrho\,, \tag{2}$$

where $D_0(C_{\mathrm{N_2}}, C_{\mathrm{H_2O}}; T)$ is the optical diffusion coefficient ($\mathrm{cm^2\,amagat/s}$) [3], ω_{J} is the resonance frequency ($\mathrm{cm^{-1}}$) of the ($\mathrm{v}=1, \mathrm{J} \rightarrow \mathrm{v}=0, \mathrm{J}$) transition, c is the speed of light (cm/s), ϱ is the density (amagat) and γ_{J}^0 is the collisional broadening coefficient ($\mathrm{cm^{-1}/amagat}$) as a function of temperature and concentrations of perturbers.

For binary mixtures, the pressure-broadening coefficients have been deduced from the inhomogeneous profile obtained through the so-called RTBT model [11]. For the ternary mixture, the inhomogeneous speed effects do not allow us to deduce pressure-broadening coefficients from the binary H_2-H_2, H_2-N_2 and H_2-H_2O mixture data with the usual mixing rule. From a rigorous point of view, a specific study of the inhomogeneous effects in the ternary system $H_2-N_2-H_2O$ should have to be performed at various concentrations and temperatures. Such a study has been recently carried out for more simple systems like H_2-Ar-N_2, $H_2-He-Ar$ and H_2-He-N_2 [12]. For $H_2-N_2-H_2O$, the situation is similar to H_2-He-N_2 since, as for the binary mixture H_2-He, experimental results have not shown any asymmetry of the H_2-H_2O line profile or any non-linearity of the measured pressure-broadening coefficients versus water concentration. Since investigations of ternary mixtures involving water have not yet been performed, and if we account for the results obtained in H_2-He-N_2 mixtures, it is reasonable to assume a homogeneous broadening for H_2O (the value of the characteristic parameter $x_{\mathrm{H_2O}}$ is thus set equal to 1 in (A2) of Appendix A, as was previously done for He [13]). As a consequence, the observed pressure-broadening coefficients of H_2-H_2O are considered as purely collisional-broadened. Then, simulations of the $\mathrm{J}=0$ to 5 Q-line profiles have been performed at 6500 points of given concentrations of hydrogen, water and nitrogen, and temperatures from 300 K to 3000 K. The pressure-broadening coefficients have been deduced from the inhomogeneous line profile and the following polynomial law has been fitted to the total map:

$$\gamma_{\mathrm{J}}^0(C_{\mathrm{N_2}},C_{\mathrm{H_2O}};T) = \gamma_{\mathrm{J}}^{\mathrm{coll}}(C_{\mathrm{N_2}},C_{\mathrm{H_2O}};T) + \gamma_{\mathrm{J}}^{\mathrm{inh}}(C_{\mathrm{N_2}},C_{\mathrm{H_2O}};T)\,, \tag{3}$$

where the collisional part obeys the usual mixing rule

$$\gamma_{\mathrm{J}}^{\mathrm{coll}}(C_{\mathrm{N_2}},C_{\mathrm{H_2O}};T) = \left(1-C_{\mathrm{N_2}}-C_{\mathrm{H_2O}}\right) \times \left(\gamma_0^{\mathrm{H_2-H_2}}+\tilde{\gamma}^{\mathrm{H_2-H_2}}T\right) + C_{\mathrm{N_2}}\left(\gamma_0^{\mathrm{H_2-N_2}}+\tilde{\gamma}^{\mathrm{H_2-N_2}}T\right) + C_{\mathrm{H_2O}}\left(\gamma_0^{\mathrm{H_2-H_2O}}+\tilde{\gamma}^{\mathrm{H_2-H_2O}}T+\tilde{\tilde{\gamma}}^{\mathrm{H_2-H_2O}}\sqrt{T}\right) \tag{4}$$

In (4) the $(\gamma_0^{\mathrm{H_2-X}}; \tilde{\gamma}^{\mathrm{H_2-X}})$ coefficients for $\mathrm{X}=\mathrm{N_2}$ and $\mathrm{H_2}$ are gathered in Table II of [5]. For $\mathrm{X}=\mathrm{H_2O}$, the coefficients $(\gamma_0^{\mathrm{H_2-X}}; \tilde{\gamma}^{\mathrm{H_2-X}}; \tilde{\tilde{\gamma}}^{\mathrm{H_2-X}})$ are given in [14]. $\gamma_{\mathrm{J}}^{\mathrm{inh}}$ is the inhomogeneous contribution to the total pressure-broadening coefficients of the ternary mixtures. It is expressed as a law

depending non-linearly on the concentration of N_2 and temperature T, and linearly on the concentration of water:

$$\gamma_{\mathrm{J}}^{\mathrm{inh}}(C_{\mathrm{N_2}}, C_{\mathrm{H_2O}}; T) = C^2{}_{\mathrm{N_2}} \left[(\tilde{a}_0)_{\mathrm{J}} + (\tilde{a}_1)_{\mathrm{J}} T + (\tilde{a}_2)_{\mathrm{J}} \sqrt{T} + C_{\mathrm{H_2O}} \left[(\tilde{a}_3)_{\mathrm{J}} + (\tilde{a}_4)_{\mathrm{J}} T + (\tilde{a}_5)_{\mathrm{J}} \sqrt{T} \right] \right], \quad (5)$$

where the $(\tilde{a}_i)_{\mathrm{J}}$ ($i = 0, 1, 2, 3, 4, 5$; $\mathrm{J} = 0, 1, 2, 3, 4, 5$) coefficients are gathered in Table 1. The error estimate between the map and the fit is less than 1%, and this functional representation provides a good description of the speed inhomogeneity. Figure 2 shows the $\gamma_{\mathrm{J}}^{\mathrm{coll}}$ (dashed lines) and γ_{J}^{0} (solid lines) coefficients for stoichiometries of 2.2 (Fig. 2a), 3.7 (Fig. 2b) and 4.1 (Fig. 2c) as a function of temperature for the three most intense H_2 lines Q(1), Q(3) and Q(5). It is evident from these figures that, for increasing stoichiometry, the mismatch between the total pressure-broadening coefficients (containing the inhomogeneous contribution) and the collisional part is getting much smaller. This is related to the amount of H_2 in the mixture, which increases with fuel-rich stoichiometry and the fact that no inhomogeneous effects exist in H_2-H_2 collisions (remember that to see a non-negligible difference between collisional and total pressure-broadening coefficients in binary H_2-N_2 mixtures the concentration of nitrogen has to be more than 40%; cf. [5, Fig. 3]). It is also worthy to note that for a stoichiometry of 2.2 (Fig. 2a) the inhomogeneous effects lead to a narrowing of the Q(1) and Q(3) lines of about 10%.

2.2 N_2 CARS spectra

Since N_2 has a small rotational constant ($B = 2\,\mathrm{cm}^{-1}$), it is not possible to simulate the Q-branch spectra at high pressure as a sum of isolated lines. Overlapping lines and intensity-transfer processes between lines play a major role in the shape of the rovibrational band. Then, the resonant part of the isotropic Q-branch spectrum is deduced from the relaxation matrix W as

$$I_{\mathrm{CARS}}^{\mathrm{N_2}} \propto \left| \chi_{\mathrm{R}}^{(3)} \right|^2 = \left| \frac{N}{\hbar} \sum_{\mathrm{J}} \alpha_{\mathrm{J}} \sum_{\mathrm{J}'} \alpha_{\mathrm{J}'} \Delta\varrho_{\mathrm{J}'} \left[G^{-1}(C_{\mathrm{N_2}}, C_{\mathrm{H_2O}}; T) \right]_{\mathrm{JJ}'} \right|^2, \quad (6)$$

with

$$G_{\mathrm{JJ}'}(C_{\mathrm{N_2}}, C_{\mathrm{H_2O}}; T) = i \left(\omega_{\mathrm{p}} - \omega_{\mathrm{S}} - \omega_{\mathrm{J}} - \delta_{\mathrm{J}}(C_{\mathrm{N_2}}, C_{\mathrm{H_2O}}; T) - i\gamma_{\mathrm{J}}(C_{\mathrm{N_2}}, C_{\mathrm{H_2O}}; T) \right) \delta_{\mathrm{JJ}'} + W_{\mathrm{JJ}'}(C_{\mathrm{N_2}}, C_{\mathrm{H_2O}}; T) \left(1 - \delta_{\mathrm{JJ}'}\right), \quad (7)$$

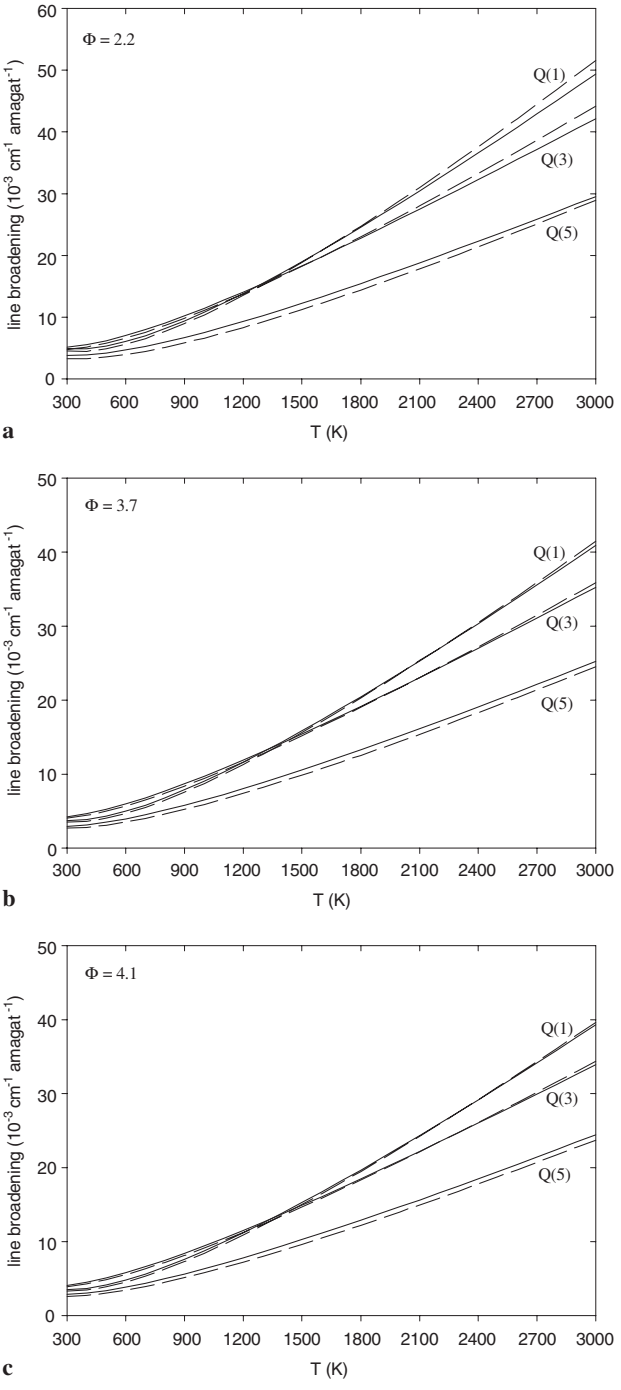

Fig. 2a–c. Behavior of γ_{J}^{0} (*solid lines*) and $\gamma_{\mathrm{J}}^{\mathrm{coll}}$ (cf. (3), *dashed lines*) for Q(1), Q(3) and Q(5) versus temperature for stoichiometries of $\Phi = 2.2$ (**a**), $\Phi = 3.7$ (**b**) and $\Phi = 4.1$ (**c**)

Table 1. Parameters $(\tilde{a}_i)_{\mathrm{J}}$ ($i = 0, 1, 2, 3, 4, 5$ and $\mathrm{J} = 0, 1, 2, 3, 4, 5$) of (5). For all fits, regression rates are above 0.99

J	Units	0	1	2	3	4	5
$\tilde{a}_0$	$10^{-3}\,\mathrm{cm}^{-1}\,\mathrm{amagat}^{-1}$	−2.019	−0.764	−2.173	−1.136	−1.77	−1.718
$\tilde{a}_1$	$10^{-6}\,\mathrm{cm}^{-1}\,\mathrm{amagat}^{-1}\,\mathrm{K}^{-1}$	−5.8	−0.3	−3.9	−1.6	−1.76	−1.67
$\tilde{a}_2$	$10^{-3}\,\mathrm{cm}^{-1}\,\mathrm{amagat}^{-1}\,\mathrm{K}^{-0.5}$	0.251	0.1615	0.333	0.221	0.284	0.293
$\tilde{a}_3$	$10^{-3}\,\mathrm{cm}^{-1}\,\mathrm{amagat}^{-1}$	−40.653	−34.4	−10.534	−29.3	−9.841	−12.024
$\tilde{a}_4$	$10^{-6}\,\mathrm{cm}^{-1}\,\mathrm{amagat}^{-1}\,\mathrm{K}^{-1}$	−109.2	−68.3	−21.3	−56.3	−18.87	−22.63
$\tilde{a}_5$	$10^{-3}\,\mathrm{cm}^{-1}\,\mathrm{amagat}^{-1}\,\mathrm{K}^{-0.5}$	3.7791	2.978	0.6619	2.414	0.671	0.909

where $\Delta\varrho_{J'}$ is the population difference between J and J′ levels. The elements of the relaxation matrix for the total mixture are deduced by employing the usual mixing rule within the N_2-N_2, N_2-H_2 and N_2-H_2O mixtures as

$$W_{JJ'}(C_{N_2}, C_{H_2O}; T) = C_{N_2} W_{JJ'}^{N_2-N_2}(T) + \left(1 - C_{N_2} - C_{H_2O}\right) W_{JJ'}^{N_2-H_2}(T) + C_{H_2O} W_{JJ'}^{N_2-H_2O}(T)\,. \quad (8)$$

The $W_{JJ'}^{N_2-X}$ ($X = N_2, H_2O$) coefficients are deduced from the well-established ECS-EP (energy corrected sudden – exponential power) model (see Appendix B and [16]) using parameters optimized for flame-temperature measurements. For $X = H_2$, no experiments are available yet to determine the ECS-EP coefficients, but semiclassical calculations of pressure-broadening coefficients have been performed using the model of [17]. The parameters of the ECS-EP model are collected in Table 2. Figure 3 shows the pressure-broadening coefficients for two temperatures (300 K and 2000 K) versus J for the N_2-N_2, N_2-H_2 and N_2-H_2O systems.

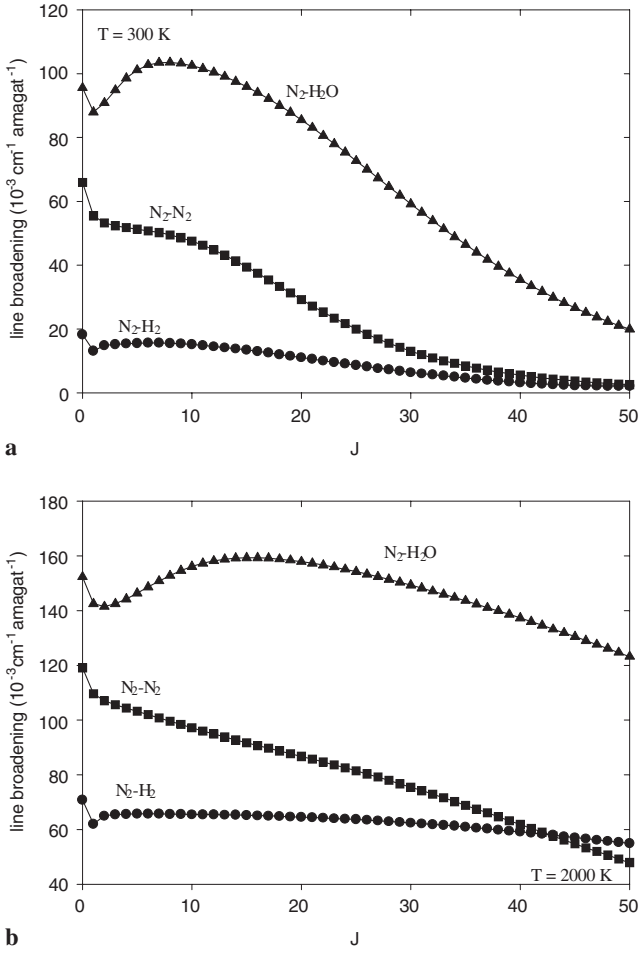

Fig. 3a,b. Behavior of N_2 pressure-broadening coefficients versus rotational quantum number J for 300 K (**a**) and 2000 K (**b**) for pure N_2 (■), N_2-H_2 (●) and N_2-H_2O (▲)

Table 2. Coefficients to calculate $W_{JJ'}$ in the ECS-EP approach for N_2-N_2, N_2-H_2O and N_2-H_2. For N_2-H_2 the ECS-EP coefficients are determined from semiclassical calculations

Coefficient	N_2-N_2	N_2-H_2O	N_2-H_2
A_0 (10^{-3} cm^{-1} amagat^{-1})	0.0206	0.0262	0.00374
γ	0.75	0.7158	0.6248
β	0.1226	0.0542	0.19055
l_c (Å)	3.5	11.4	1.95
M	2.051	–	–
N	–	1.155	0.7042

3 Results and discussion

3.1 Determination of reference temperature

The main purpose of this work has been the determination of the accuracy of H_2 CARS thermometry by taking into account the influence of N_2 and, in particular, of H_2O as colliding partners for the hydrogen molecule. The reliability of the evaluated H_2 CARS temperatures has been checked by an independent temperature measurement from N_2. Such a comparison was applied in atmospheric-pressure hydrogen/air flames ($\Phi = 0.5$ to 2.5) by Hancock et al. [1]. Here the temperature from H_2 CARS Q-branch spectra was determined by a line-integrated Boltzmann plot and was compared to N_2 CARS values deduced from a theory–experiment fit. The accuracy of N_2 CARS temperatures was stated to be about 1–2%. A systematic mismatch between the H_2 and N_2 temperatures was observed for fuel-rich conditions, which was primarily attributed to uncertainties in H_2 line widths. Usually, N_2 CARS thermometry is applied to air-fed hydrocarbon flames. In these flames the concentration of hydrogen in the probe volume is negligible and, therefore, hydrogen has not been taken into account in the evaluation procedure, but has to be considered in fuel-rich flames. In our investigation, for experimental reasons, we burnt fuel-rich ($\Phi \cong 4$) H_2/air flames. Thus, the remaining amount of H_2 in the exhaust gas was in the range of about 50%. Consequently, the influence of H_2 could not be neglected a priori. Thus, we implemented the calculated N_2-H_2 line-broadening coefficients in our N_2 CARS evaluation program.

Since the N_2-H_2 coefficients are not verified by experiments, we had to be careful with the interpretation of the temperatures yielded with the modified N_2 CARS evaluation program. Tests were made to insure the plausibility of our results. First of all we analyzed the N_2 Q-branch data ignoring the influence of H_2, i.e. using the unmodified evaluation routines and parameters. All H_2-specific parameters are assumed to be the same as for N_2. Then, we also took the N_2-H_2 linewidth contribution into account. A comparison of these two results is shown in Fig. 4. Neglecting the N_2-H_2 coefficients in the analysis leads to some rise of the temperature. This can be explained by looking at the curves of Fig. 3. The N_2-N_2 coefficients are larger than the N_2-H_2 coefficients. Using too large line widths in the evaluation code yields higher temperatures, but still within the estimated error of about 4% for an averaged spectrum, indicating that the influence of hydrogen as collider for the evaluation of N_2 CARS spectra is small. Some uncertainty of the N_2-H_2 line-broadening coefficients has only a slight influence on the accuracy of the N_2 CARS temperature.

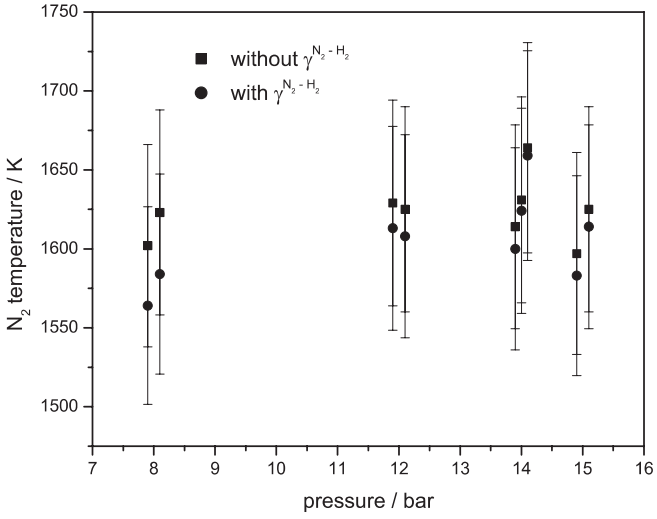

Fig. 4. Comparison of N_2 temperature evaluation ($\Phi = 4.1$) taking into account the N_2-H_2 line-width contribution and neglecting it. The *bars* indicate an error of ±4%

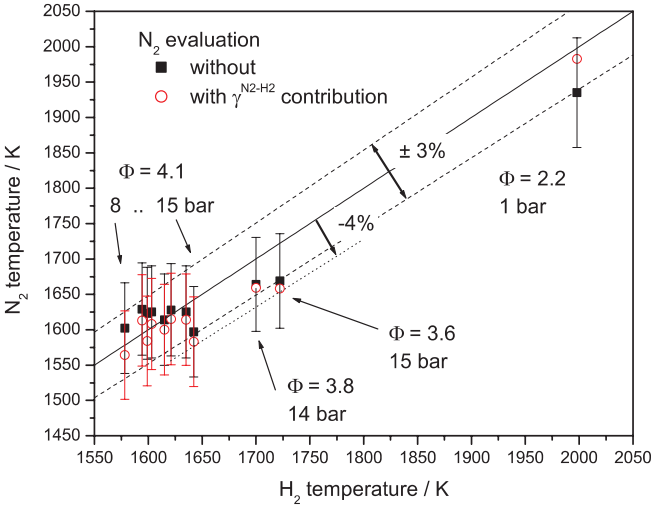

Fig. 5. Comparison of H_2 and N_2 temperatures

3.2 Comparison of temperatures determined by N_2 and H_2 CARS

For the fundamental investigation of the accuracy of H_2 CARS thermometry at high pressure, the stability and reproducibility of the flame is important. Before starting the experiment, the H_2/air flame was characterized by recording an axial temperature profile with N_2 CARS. The flame front was 0.5 mm above the burner matrix and a temperature gradient of 20–40 K/mm was observed for the height of 1 to 4 mm above the burner, probably caused by H_2 afterburning. All measured temperatures were slightly below the adiabatic flame temperature calculated for a temperature of 400 K of the unburnt gases. The evaluation of N_2 single-pulse temperatures did not reveal any temporal drift or temperature spikes over a test period of 2 min, which would indicate instabilities of the flame or problems caused by the entrainment of cold co-flowing air. The measurements to compare H_2 and N_2 CARS temperatures were performed at a height of 3 mm above the matrix. The pressure was varied between 8, 10, 12, 14 and 15 bar, while the stoichiometry was $\Phi = 4.1$. As mentioned above, the range of stability of the flame was small; thus only for 14 bar ($\Phi = 3.6$) and 15 bar ($\Phi = 3.8$) was a variation of the stoichiometry possible. Additionally, a single test point was measured at 1 bar, where the H_2 line widths are purely Doppler-determined and pressure broadening can be neglected. The comparison of the temperatures resulting from H_2 and N_2 CARS is shown in Fig. 5. The conservatively estimated error of the N_2 CARS temperatures is about 4%. Most of the H_2 temperatures are in the range of ±3%.

To investigate the influence of the different contributions of the H_2 line widths on the evaluated H_2 temperature, different approaches of data analysis were performed by modifying the contributing portions of the various linewidth coefficients. First, the H_2 Q-branch spectra were evaluated using pure Doppler broadening, which is equivalent to a Boltzmann-plot analysis. Both pressure broadening and Dicke narrowing was neglected (→ Doppler). Second, the pressure-broadened line widths were set to pure self-broadening of H_2, neglecting the N_2 as well as the H_2O contributions (→ pure H_2). Next, the H_2O (→ without H_2O) and the N_2 contributions (→ without N_2) were disregarded. Last, the total RTBT correction term (γ^{inh}, cf. (3), → pure collisional) was set to zero or only the H_2O contribution of this correction term (→ without H_2O in RTBT). The temperature changes due to these variations are plotted in Fig. 6. The zero line indicates the temperature yielded with the full set of coefficients. At 1 bar and at a temperature of about 2000 K (corresponding to 0.15 amagat) the line widths are settled by Doppler broadening. If Dicke narrowing is assumed in the evaluation procedure, a temperature decrease of about 50 K is obtained. In the high-pressure regime, the description of the line widths as purely Doppler-broadened leads to the strongest deviations in the temperature. The degree of deviation grows with increasing pressure due to the increasing influence of pressure broadening. The deviations caused by taking into account only self-broadening of hydrogen or by ignoring the water contribution are up to 15%, even at moderate densities (2.5 amagat). The influence of nitrogen on the H_2 CARS temperature is only about one-third of that of water, but the sign is reversed. The temperature changes generated by neglecting the correction terms of the polynomial RTBT approximation are

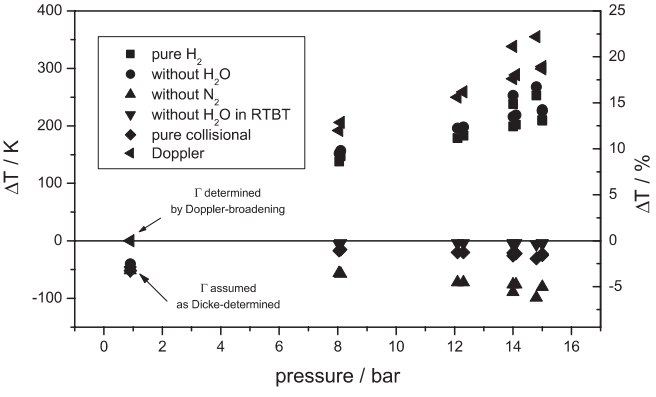

Fig. 6. Temperature mismatch ($\Delta T = T_{variation} - T_{H_2}$) as a function of pressure by taking several contributions of the broadening coefficients. Experimental data at 15 bar correspond to density of approx. 2.5 amagat

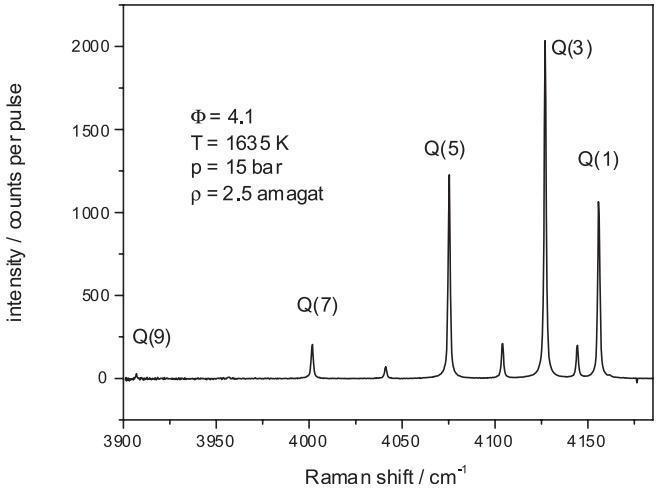

Fig. 7. Averaged Q-branch H_2 CARS spectrum

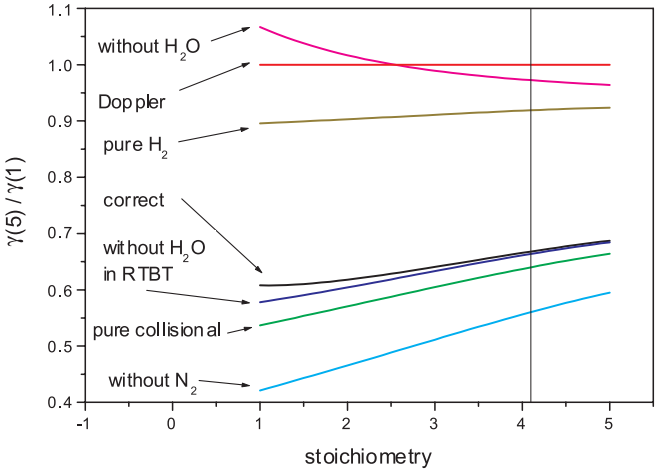

Fig. 8. Ratio ${\gamma^0}_5/{\gamma^0}_1$ as a function of stoichiometry at adiabatic flame temperature. The experimental stoichiometry is $\Phi = 4.1$

small, i.e. less than 2%. Because of the widespread lines in the H_2 Q-branch spectrum (Fig. 7), the temperature information depends largely on the spectral fit of a few lines with high intensity. For the temperature level in this experiment of around 1620 K, the most intense lines are Q(1), Q(3) and Q(5). A variation of the line widths of all three lines by 10% has a very slight influence on the resulting temperature, in contrast to a variation of the ratio of the line-width coefficients of Q(5) and Q(1). To illustrate this, the ratio ${\gamma^0}_5/{\gamma^0}_1$ is plotted in Fig. 8.

4 Conclusion

In this work a detailed study was performed to identify the influence of the line widths on the accuracy of temperature from H_2 CARS spectra in high-pressure flames. Based on an earlier study [5], where the influence of nitrogen as collider was investigated in binary H_2-N_2 mixtures, CARS measurements were now carried out in hydrogen/air flames under various conditions. Besides the H_2 CARS measurements, N_2 CARS thermometry was employed to get an independent reference temperature. To achieve high accuracy of temperature the consideration of the line widths of the indicator molecule is important, for H_2 and N_2 CARS as well. Usually, in air-fed hydrocarbon combustion the concentration of H_2 is low and its influence can be neglected, which is not the case in fuel-rich H_2/air flames. High concentrations of H_2 in the exhaust require that the contribution of N_2-H_2 collisions to the total line widths has to be accounted for in the analysis of the N_2 CARS spectra. While the former study dealt with H_2 CARS thermometry in binary mixtures, here ternary mixtures of $H_2-H_2O-N_2$ had to be considered. Therefore, the theoretical description of the H_2-N_2 line widths (RTBT) had to be extended by the additional contribution of H_2O. As pointed out in our previous work, the influence of the line widths on the evaluated temperature is mainly determined by the line-width ratio of the most intense lines (here Q(1), Q(3) and Q(5)). The temperature error found by neglecting distinct line-width contributions can reach several tens of percent. Therefore, the use of the correct line widths is recommended for accurate temperature measurements with H_2 CARS in high-pressure combustion.

Acknowledgements. We gratefully acknowledge the support of this work by a grant from the Deutscher Akademischer Austauschdienst (DAAD) and the Ministère des Affaire Etrangères (MAE) in the frame of PROCOPE. The authors would also like to thank H. Berger, X. Michaut and R. Saint-Loup (Laboratoire de Physique, Dijon) for providing us with the H_2-H_2O data prior to publication and H. Eberius (DLR) for experimental support.

Appendix

A The extended ternary mixture RTBT line-shape model

The so-called RTBT speed-dependent line-shape model [17] can be expressed as

$$\mathrm{Im}\left\{\chi_{\mathrm{R}}^{(3)}\right\} \propto \frac{N}{\hbar^3}\sum_{\mathrm{J}}\pi^{-1} \times \mathrm{Re}\left\{\frac{\alpha_{\mathrm{J}}^2 g_{\mathrm{J}}\,(2\mathrm{J}+1)\,\mathrm{e}^{-E_{\mathrm{J}}/kT}\left(1-\mathrm{e}^{E_{\mathrm{v}=1}/kT}\right)\langle[\mathrm{i}\tilde{\omega}+F(v)]^{-1}\rangle}{1-\langle[x\nu_{\mathrm{coll}}-x\gamma_{\mathrm{coll}}(v)-\mathrm{i}x\delta_{\mathrm{coll}}(v)]\,[\mathrm{i}\tilde{\omega}+F(v)]^{-1}\rangle}\right\} \tag{A.1}$$

where $F(v) = x\nu_{\mathrm{coll}} + (1-x)\gamma_{\mathrm{coll}}(v) + i(1-x)\delta_{\mathrm{coll}}(v)$, $\langle\ldots\rangle$ means the average over the absolute radiator speed v, $\tilde{\omega} = \omega_{\mathrm{J}} - \omega_{\mathrm{P}} + \omega_{\mathrm{S}}$, $\gamma_{\mathrm{coll}}(v)$ and $\delta_{\mathrm{coll}}(v)$ denote the v-dependent line broadening and line shifting and ν_{coll} the total collision frequency. The parameter x is the fraction of collisions inducing speed-class exchanges. The linear dependence of $x\nu_{\mathrm{coll}}$, $x\gamma_{\mathrm{coll}}$, $x\delta_{\mathrm{coll}}$, $(1-x)\gamma_{\mathrm{coll}}$ and $(1-x)\delta_{\mathrm{coll}}$ versus perturber concentration allows one to extend the RTBT model for the case of three collisional partners [12] (within the impact approximation). One obtains a set of expressions of the form

$$x\nu_{\mathrm{coll}} = c_{\mathrm{H_2}}\,x_{\mathrm{H_2-H_2}}\,\nu_{\mathrm{coll/H_2-H_2}} + c_{\mathrm{N_2}}\,x_{\mathrm{H_2-N_2}}\,\nu_{\mathrm{coll/H_2-N_2}} + c_{\mathrm{H_2O}}\,x_{\mathrm{H_2-H_2O}}\,\nu_{\mathrm{coll/H_2-H_2O}}\,, \tag{A.2}$$

(similar laws hold for $x\nu_{\mathrm{coll}}$, $x\gamma_{\mathrm{coll}}$, $x\delta_{\mathrm{coll}}$, $(1-x)\gamma_{\mathrm{coll}}$ and $(1-x)\delta_{\mathrm{coll}}$).

For all the binary H_2-X mixtures, the collisional parameters exhibit a temperature dependence [14] which is well represented by

$$\gamma_{\text{coll}}(T) \text{ or } \delta_{\text{coll}}(T) = AT + B\sqrt{T} + C\,. \tag{A.3}$$

The values of the A, B and C factors (for both broadening and shifting) are given for H_2-H_2, H_2-N_2 in [4] and those for H_2-H_2O in [14]. The H_2 speed dependence of the collisional partners $\gamma_{\text{coll}}(v)$ and $\delta_{\text{coll}}(v)$ in (A.1) is deduced from (A.3) by means of the method previously developed in [18, 19].

B The ECS-EP law

The ECS scaling law [15] gives the relaxation-matrix elements between an initial rotational state J and a final state J′. These elements are written as

$$-\text{Re}W_{\text{JJ}'}^{\text{ECS-EP}}(T) = (2\text{J}'+1)\exp\left(\left(E_{\text{J}'} - E_{\text{J}_>}\right)/kT\right)\Omega_{\text{J}_>}^2 \times \sum_{\text{L}} \begin{pmatrix} \text{J} & \text{J}' & \text{L} \\ 0 & 0 & 0 \end{pmatrix}^2 (2\text{L}+1)\Omega_{\text{L}}^{-2}\frac{A(T)}{[\text{L}(\text{L}+1)]^{\nu}}\exp\left(-\beta E_{\text{L}}/kT\right)\,, \tag{B.1}$$

where $\text{J}_>$ is the greater value of J or J′, E_{J} is the rotational energy of the level J, (:::) is a 3-J coupling symbol and Ω_{J} is the adiabatic factor which introduces a correction to take into account the rotation of the molecule during the collision. It is given by

$$\Omega_{\text{J}} = \frac{1}{1+\frac{\omega_{\text{J,J}-2}^2 l_{\text{c}}^2}{24\bar{v}_{\text{rel}}^2}}\,, \tag{B.2}$$

where l_{c} is the interaction length, $\omega_{\text{J,J}-2}$ the internal level spacing of the optically active molecule and $\bar{v}_{\text{rel}}$ the mean relative thermal velocity. For pure N_2 [16], the amplitude parameter $A(T)$ is modeled, in contrast to [15], as

$$A(T) = A_0\frac{1-\text{e}^{-m}}{1-\text{e}^{-mT/T_0}}\,, \tag{B.3}$$

where T_0 is room temperature. For N_2-H_2O it follows the power law introduced by Bonamy et al. [20]:

$$A(T) = A_0\left(\frac{T_0}{T}\right)^{N-1}\,. \tag{B.4}$$

All constants used to calculate the CARS spectra of N_2 are gathered in Table 2.

References

1. R.D. Hancock, K.E. Bertagnolli, R.P. Lucht: Combust. Flame **109**, 323 (1997)
2. V. Bergmann, M. Woyde, W. Stricker: In *Coherent Raman Spectroscopy: Application and New Developments*, ed. by E.M. Castellucci, R. Righini, P. Foggi (World Scientific, Singapore 1993) p. 153
3. V. Bergmann, W. Stricker: Appl. Phys. B **61**, 49 (1995)
4. P.M. Sinclair, J.Ph. Berger, X. Michaut, R. Saint-Loup, R. Chaux, H. Berger, J. Bonamy, D. Robert: Phys. Rev. A **54**, 402 (1996)
5. J. Hussong, W. Stricker, X. Bruet, P. Joubert, J. Bonamy, D. Robert, X. Michaut, T. Gabard, H. Berger: Appl. Phys. B **70**, 447 (2000)
6. R. Lückerath, M. Woyde, W. Meier, W. Stricker, U. Schnell, H.-Ch. Magel, J. Görres, H. Spliethoff, H. Maier: Appl. Opt. **34**, 3303 (1995)
7. A.C. Eckbreth: *Laser Diagnostics for Combustion, Temperature and Species* (Overseas Publisher Association, Amsterdam 1996)
8. A. Roblin: Thesis, Université de Rouen, France (1990)
9. R.H. Dicke: Phys. Rev. **89**, 472 (1953)
10. J.P. Wittke, R.H. Dicke: Phys. Rev. **103**, 620 (1956)
11. D. Robert, J.M. Thuet, J. Bonamy, S. Temkin: Phys. Rev. A **47**, 771 (1993)
12. P. Joubert, X. Bruet, J. Bonamy, D. Robert, F. Chaussard, R. Saint-Loup, H. Berger: J. Chem. Phys. **113**, 10056 (2000)
13. J.W. Forsman, J. Bonamy, D. Robert, J.Ph. Berger, R. Saint-Loup, H. Berger: Phys. Rev. A **52**, 2652 (1995)
14. X. Michaut: Thesis, Université de Bourgogne, France (1999)
15. G. Millot: J. Chem. Phys. **93**, 8001 (1990)
16. M. Fischer, E. Magens, H. Weisgerber, A. Winandy, S. Cordes: AIAA J. **37**, 744 (1999)
17. D. Robert, J. Bonamy: J. Phys. (Paris) **40**, 923 (1979)
18. H. Pickett: J. Chem. Phys. **73**, 6090 (1980)
19. J.Ph. Berger: Thesis, Université de Bourgogne, France (1994)
20. L. Bonamy, J. Bonamy, D. Robert, B. Lavorel, R. Saint-Loup, R. Chaux, J. Santos, H. Berger: J. Chem. Phys. **89**, 5568 (1988)